Role of OH-stretch/torsion coupling and quantum yield effects in the first OH overtone spectrum of cis-cis HOONO

Anne B. McCoy, Juliane L. Fry, Joseph S. Francisco, Andrew K. Mollner, and Mitchio Okumura

Citation: The Journal of Chemical Physics **122**, 104311 (2005); doi: 10.1063/1.1859273
View online: http://dx.doi.org/10.1063/1.1859273
View Table of Contents: http://scitation.aip.org/content/aip/journal/jcp/122/10?ver=pdfcov
Published by the AIP Publishing

Role of OH-stretch/torsion coupling and quantum yield effects in the first OH overtone spectrum of *cis-cis* HOONO

Anne B. McCoy[a)]
Department of Chemistry, The Ohio State University, Columbus, Ohio 43210

Juliane L. Fry
Arthur Amos Noyes Laboratory of Chemical Physics, California Institute of Technology, Pasadena, California 91125

Joseph S. Francisco
Department of Chemistry, Purdue University, West Lafayette, Indiana 47907

Andrew K. Mollner and Mitchio Okumura[b)]
Arthur Amos Noyes Laboratory of Chemical Physics, California Institute of Technology, Pasadena, California 91125

(Received 24 November 2004; accepted 21 December 2004; published online 11 March 2005)

A joint theoretical and experimental investigation is undertaken to study the effects of OH-stretch/HOON torsion coupling and of quantum yield on the previously reported first overtone action spectrum of *cis-cis* HOONO (peroxynitrous acid). The minimum energy path along the HOON dihedral angle is computed at the coupled cluster singles and doubles with perturbative triples level with correlation consistent polarized quadruple ζ basis set, at the structure optimized using the triple ζ basis set (CCSD(T)/cc-pVQZ//CCSD(T)/cc-pVTZ). The two-dimensional *ab initio* potential energy and dipole moment surfaces for *cis-cis* HOONO are calculated as functions of the HOON torsion and OH bond length about the minimum energy path at the CCSD(T)/cc-pVTZ and QCISD/AUG-cc-pVTZ (QCISD—quadratic configuration interaction with single and double excitation and AUG-augmented with diffuse functions) level of theory/basis, respectively. The OH-stretch vibration depends strongly on the torsional angle, and the torsional potential possesses a broad shelf at ~90°, the *cis-perp* conformation. The calculated electronic energies and dipoles are fit to simple functional forms and absorption spectra in the region of the OH fundamental and first overtone are calculated from these surfaces. While the experimental and calculated spectra of the OH fundamental band are in good agreement, significant differences in the intensity patterns are observed between the calculated absorption spectrum and the measured action spectrum in the $2\nu_{OH}$ region. These differences are attributed to the fact that several of the experimentally accessible states do not have sufficient energy to dissociate to $OH+NO_2$ and therefore are not detectable in an action spectrum. Scaling of the intensities of transitions to these states, assuming $D_0=82.0$ kJ/mol, is shown to produce a spectrum that is in good agreement with the measured action spectrum. Based on this agreement, we assign two of the features in the spectrum to $\Delta n=0$ transitions (where n is the HOON torsion quantum number) that are blue shifted relative to the origin band, while the large peak near 7000 cm^{-1} is assigned to a series of $\Delta n=+1$ transitions, with predominant contributions from torsionally excited states with substantial *cis-perp* character. The direct absorption spectrum of *cis-cis* HOONO (6300–6850 cm^{-1}) is recorded by cavity ringdown spectroscopy in a discharge flow cell. A single band of HOONO is observed at 6370 cm^{-1} and is assigned as the origin of the first OH overtone of *cis-cis* HOONO. These results imply that the origin band is suppressed by over an order of magnitude in the action spectrum, due to a reduced quantum yield. The striking differences between absorption and action spectra are correctly predicted by the calculations. © *2005 American Institute of Physics*. [DOI: 10.1063/1.1859273]

I. INTRODUCTION

Peroxynitrous acid, HOONO, is a weakly bound isomer of nitric acid that is formed as a secondary product of the reaction:

$$OH + NO_2 + M \rightarrow HONO_2 + M, \quad \Delta_{1a}H^0(0) = -204 \text{ kJ/mol}, \tag{1a}$$

$$OH + NO_2 + M \rightarrow HOONO, \quad \Delta_{1b}H^0(0) = -82.0 \text{ kJ/mol}. \tag{1b}$$

Reaction (1a) is a critical radical chain termination step in the atmosphere, as OH and NO_2 combine to form stable

[a)]Author to whom correspondence should be addressed. Electronic mail: mccoy@chemistry.ohio-state.edu
[b)]Author to whom correspondence should be addressed. Electronic mail: mo@caltech.edu

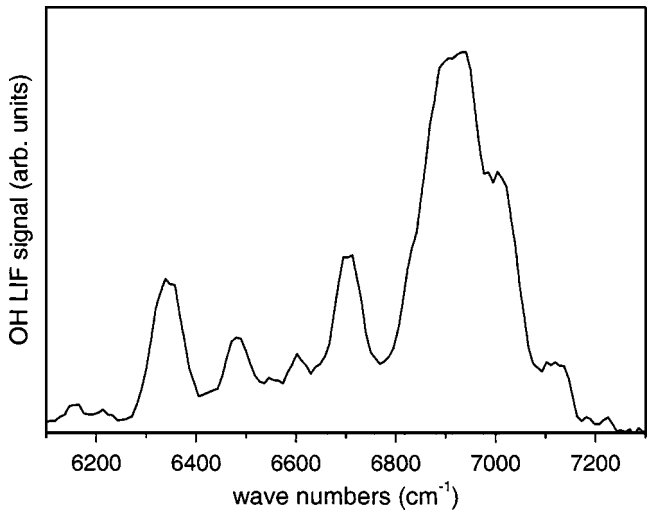

FIG. 1. Smoothed action spectrum of the first overtone of the OH stretch ($2\nu_{OH}$) band in *cis-cis* HOONO, recorded at 10 Torr, 300 K (Refs. 1 and 6).

nitric acid. Channel (1b) reduces the efficacy of reaction (1a) as a sink of HO_x and NO_x radicals, because HOONO rapidly redissociates under atmospheric conditions. HOONO has been the focus of many studies in the past two decades, but only recently has there been direct evidence for its existence and formation in the gas phase under thermal conditions.[1–4]

Theoretical studies establish the stability of HOONO and have identified several minima and transition states. The lowest energy conformer is *cis-cis* HOONO, a planar ring structure in which the OH forms a weak intramolecular hydrogen bond with the terminal O atom. The *trans-perp* conformer, with the heavy atoms in a plane in a *trans* configuration and the OH bond perpendicular to that plane, has been predicted to lie 15.3 kJ/mol (1280 cm^{-1}) higher in energy at the CCSD(T)/cc-pVTZ level of theory.[5,6]

A third postulated minimum corresponds to the *cis-perp* geometry in which the heavy atoms are in a plane in a *cis* configuration and the OH bond is perpendicular to that plane. This conformer was first investigated by McGrath and Rowland at the MP2/6-311+G(3*df*,2*p*) (MP2–Møller-Plesset perturbation theory truncated at the second order) level of theory,[7] and has since been studied by several groups at various levels of theory.[4,8–12] The calculations of Golden *et al.* at the QCISD(T)/cc-pVDZ level[5] (QCISD—quadratic configuration interaction with single and double excitation) and Bean *et al.* at the CCSD(T)/cc-pVTZ level[2] demonstrate that higher levels of theory are required for a good description of HOONO. Attempts to locate a *cis-perp* HOONO minimum at the CCSD(T) level have been unsuccessful,[5,6,13] calling into question earlier predictions of a *cis-perp* minimum. In the first spectroscopic detection of HOONO, Lee and co-workers reported matrix-isolation spectra of two of the HOONO isomers, *cis-cis* and *trans-perp* HOONO, but did not observe the *cis-perp* isomer.[14,15]

Recently, Nizkorodov and Wennberg reported the first direct spectroscopic detection of HOONO in the gas phase,[1] reproduced in Fig. 1. In this experiment, excitation of HOONO in the near infrared at the first OH stretch overtone ($2\nu_{OH}$) region was detected by monitoring OH products from vibrational predissociation. The observed spectrum was unusual, with a series of broad peaks from 6300 to 7200 cm^{-1}. A peak at 6365 cm^{-1} was identified as the $2\nu_{OH}$ origin, but the spectrum was dominated by a large, partially blended peak at 6970 cm^{-1}. Nizkorodov and Wennberg tentatively assigned the peaks based on *ab initio* predictions to all three conformers of HOONO, but the lack of observable structure did not allow a definitive assignment.

More recent studies have shown that *trans-perp* HOONO has a spectrum distinct from that shown in Fig. 1,[6,16] and isomerizes quickly to the more stable *cis-cis* conformer (millisecond time scale at room temperature and ~10 Torr).[6] Fry *et al.* therefore attribute all of the bands reported by Nizkorodov and Wennberg to the lowest energy conformer, *cis-cis* HOONO. Matthews *et al.*[17] conclude that the strong 6970 cm^{-1} band is due to *trans-perp* HOONO; however, this is at odds with the experimental observations of Fry *et al.*

The appearance of the action spectrum of HOONO is unusual. A typical overtone spectrum comprises a strong origin band and weaker satellite features; the weak bands are either combination bands (including Fermi Resonances) or hot bands (including sequence bands). The majority of the oscillator strength is typically carried in the local $2\nu_{OH}$ mode. Any assignment of the *cis-cis* HOONO overtone spectrum must explain why this origin band is relatively weak.

One factor that may be important in understanding the anomalous intensity pattern of the overtone action spectrum is the wavelength dependence of the quantum yield. The quantum yield is unity if the photon energy is greater than the dissociation energy D_0. Konen *et al.* now estimate a D_0 for *cis-cis* HOONO of 82.0 kJ/mol (6860 cm^{-1}).[18] All of the bands in the action spectrum that are below the dissociation threshold of 6860 cm^{-1} must be hot bands. Rice–Ramsperger–Kassel–Marcus (RRKM) calculations by Fry *et al.* indicate that the quantum yield falls off rapidly below this limit.[6] Thus, the intensity of bands at frequencies below D_0 would be suppressed.

A second feature of *cis-cis* HOONO that may be responsible for the anomalous intensity patterns is the presence of an intramolecular hydrogen bond, which couples the OH stretch with low-frequency, large amplitude modes near the equilibrium configuration. The internal hydrogen bond causes a redshift in the OH-stretch frequency in *cis-cis* HOONO, with an observed fundamental frequency of 3306 cm^{-1};[2] based on the expected anharmonic correction, the origin of the *cis-cis* HOONO first overtone is the 6365 cm^{-1} band. Torsional motion about the OO bond (the HOON dihedral angle, here referred to as τ) will break the hydrogen bond and lead to a blueshift of the OH bond frequency back to ≈3530 cm^{-1}. The intensity of the OH stretch is predicted to be weaker in the hydrogen-bonded form, by a factor of 1.5 in the double harmonic approximation (QCISD/AUG-cc-pVDZ). Thus, torsionally excited molecules, in which the hydrogen bond is effectively broken, may have absorption bands that are blueshifted and possess larger cross sections than the *cis-cis* HOONO origin.

The above considerations lead to the following hypothesis. The overtone action spectrum observed by Nizkorodov

and Wennberg (Fig. 1) is that of *cis-cis* HOONO, but the relative band intensities deviate significantly from the expected absorption spectrum due to quantum yield effects. The origin and combination bands below D_0 will appear weak, because they have a reduced quantum yield for dissociation. The strong bands at 6970 cm^{-1} arise from hot, torsionally excited molecules for which the internal hydrogen bond has been broken, resulting in a vibrationally averaged frequency of the OH bond close to that of a free OH stretch. The pure absorption spectrum will possess a strong origin band, but will still have significant hot bands and sequence bands with large spectral shifts to the blue that arise from strong coupling between the OH stretch and the low-frequency torsional modes, particularly the HOON torsion.

The present work is a joint theoretical and experimental effort to investigate this hypothesis. We have calculated the absorption and action spectra of *cis-cis* HOONO in the fundamental and first overtone region from first principles, using a two-dimensional model that explicitly treats the OH stretch and HOON torsional degrees of freedom, and experimentally measured the first overtone spectrum of HOONO in direct absorption.

(i) An *ab initio* minimum energy path along the HOON torsional coordinate τ was generated at the CCSD(T)/cc-pVTZ level with the OONO dihedral angle frozen so that the heavy atoms lie in a plane. CCSD(T) energies were also calculated with a cc-pVQZ basis set at the same nuclear geometries. This calculation provides the most accurate prediction to date of the HOON torsional potential, including the *cis-perp* HOONO conformer.

(ii) Electronic energies and the dipole moment components were calculated as functions of the OH stretch coordinate r for fixed HOON angles τ at the CCSD(T)/ccpVTZ and QCISD/AUG-cc-pVTZ level of theory/basis, respectively.

(iii) Two-dimensional quantum mechanical calculations were performed to solve for the torsion-vibration energy levels and transition moments from the resulting surfaces.

(iv) Both absorption and action spectra at 300 K were calculated. The action spectrum was predicted by convoluting the calculated absorption spectrum with a simplified quantum yield. The temperature dependence of this action spectrum was investigated by calculating spectra at 233 and 300 K.

(v) The absorption spectrum was recorded in the region 6300–6800 cm^{-1} by cavity ringdown spectroscopy and compared to the experimental action spectrum and to the theoretical predictions.

II. THEORETICAL AND COMPUTATIONAL METHODS

A. Torsional potential

In order to investigate the role of torsional motion in the *cis-cis* HOONO spectrum in the region of the first overtone, we first calculated a one-dimensional potential surface $V^{\mathrm{MEP}}(\tau)$. This surface is a minimum energy path through the HOONO surface, as a function of the HOON torsion angle τ evaluated at increments of 10°. The OONO dihedral angle was fixed to 0° (the *cis* configuration) and the values of the remaining seven internal coordinates were optimized to minimize the total energy. The potential was calculated using the coupled-cluster method with single and double excitations which incorporated a perturbative estimate of the effects of connected triple excitations [CCSD(T)].[19–21] The Dunning correlation consistent cc-pVTZ basis set was used.[22–24] The Hessian from a quadratic configuration interaction with single and double excitation (QCISD) method[25] optimization of the geometry was used for the geometry optimization at the CCSD(T) level. The energies along the minimum energy path were also calculated at the CCSD(T)/cc-pVQZ level for the geometries previously optimized at the CCSD(T)/cc-pVTZ level of theory and basis set. To distinguish between these two minimum energy paths, we denote them by $V^{\mathrm{MEP}}_{\mathrm{pVTZ}}(\tau)$ and $V^{\mathrm{MEP}}_{\mathrm{pVQZ}}(\tau)$, respectively. The GAUSSIAN98 program[26] was used in all the calculations.

B. Two-dimensional torsion-stretch potential energy and dipole surfaces

To explore further the vibrational states of *cis-cis* HOONO, two-dimensional potential and dipole moment surfaces were evaluated as functions of r and τ, with the remaining seven coordinates constrained to their values on the minimum energy path surface. The potential points were evaluated at the CCSD(T)/cc-pVTZ level of theory/basis set, while the dipole moment surface was evaluated at the QCISD/AUG-cc-pVTZ level of theory/basis set. The potential and dipole surfaces were evaluated for 13 angles and 13 OH distances. The values of r ranged from $r_e(\tau)-0.3$ Å to $r_e(\tau)+0.3$ Å, where $r_e(\tau)$ is the value of the OH bond length along the minimum energy surface at the specified value of τ. The values of τ that were used to construct the two-dimensional surface were 0°, 10°, 20°, 30°, 40°, 60°, 70°, 80°, 90°, 100°, 120°, 150°, and 180°. These points were chosen to span the range of this angle [by symmetry $V(r,\tau)=V(r,-\tau)$] with a higher density of points near the potential minimum and the *cis-perp* conformation.

To correct for the small differences in the energies obtained with the cc-pVQZ and cc-pVTZ basis sets along the minimum energy path, for each value of τ the energies were scaled by $\sigma(\tau)$, the ratio of the energy differences computed by the two basis sets:

$$V(r,\tau)=V_{\mathrm{pVTZ}}(r,\tau)\left[\frac{V^{\mathrm{MEP}}_{\mathrm{pVQZ}}(\tau)-V^{\mathrm{MEP}}_{\mathrm{pVQZ}}(0°)}{V^{\mathrm{MEP}}_{\mathrm{pVTZ}}(\tau)-V^{\mathrm{MEP}}_{\mathrm{pVTZ}}(0°)}\right]$$
$$=V_{\mathrm{pVTZ}}(r,\tau)\sigma(\tau). \quad (2)$$

As $\sigma(\tau)$ is not defined at $\tau=0°$, we extrapolated the scaling from its values at 10°, 20°, and 30° and used $\sigma(0°)=0.943$.

The one-dimensional slices along r through the unscaled cc-pVTZ basis potential at each value of τ were fit to a Morse oscillator,

$$U_{\mathrm{pVTZ}}(r,\tau)=D_e(\tau)[1-\exp(-\alpha(\tau)[r-r_e(\tau)])]^2+U_e(\tau), \quad (3)$$

in order to facilitate extrapolation to a larger range of OH distances. In these fits, all parameters were allowed to vary. Evaluation of the full scaled potential $U(r,\tau)$ was achieved by multiplying $D_e(\tau)$ and $U_e(\tau)$ by the appropriate scaling

factor $\sigma(\tau)$, and using a cubic spline interpolation to evaluate these potential parameters at intermediate angles. The scaled versions of the parameters will be denoted as $D_e^{(s)}(\tau)$ and $U_e^{(s)}(\tau)$ in the discussion that follows. For the spline, the grid was extended to $-360°$ through 360° by symmetry in order to avoid unphysical edge effects.

A similar approach was employed to fit the dipole moment surface. Here we first transformed the dipole moment operator into the principal-axis system for the four heavy atoms. We then fit each of the three Cartesian components of the dipole moment to a cubic polynomial in $[r-r_e(\tau)]$. The form of the surface and the resulting intensities will depend on the choice of the embedding of the body-fixed axis system. A principal-axis system was selected in which the three principal axes were determined at each of the 13 geometries along the minimum energy path and the axes are labeled to ensure that the rotational constants obey $A>B>C$. Since the transformation is based on the four heavy atoms, which do not move significantly over the full range of τ, we find that the rotational constants vary by no more than 5%. This is much smaller than the differences between the rotational constants. Evaluation of the vector components of the dipole moment surface was achieved by spline interpolation of the fit parameters.

C. Vibrational energy levels, transition intensities, and spectra

Having obtained a potential and dipole moment surface, the energies and intensities were determined using a two-dimensional discrete variable representation method,[27,28] where both the radial and angular dependences are treated on evenly spaced grids of points with 30 and 75 points, respectively. The value of τ was allowed to vary from $-180°$ to 180°, while r ranged from 0.500 to 2.225 Å. With these energies and wave functions, the transition strengths of the lines were evaluated using

$$I_{v'',n'';v',n'}(\nu) = \nu|\langle v'n'|\boldsymbol{\mu}(r,\tau)|v''n''\rangle|^2, \tag{4}$$

where ν is the transition wave number in cm^{-1} and $\boldsymbol{\mu}$ is the dipole moment in D, and v and n are the quantum numbers for OH stretch and torsion, respectively. The intensities of lines in the absorption spectrum can then be determined by multiplying the transition strength by a Boltzmann factor $f_{v'',n''}(T)$ accounting for the population of the lower state in the transition,

$$I_{\mathrm{ABS}v'',n'';v',n'}(\nu,T) = C \times f_{v'',n''}(T) \times I_{v'',n'';v',n'}(\nu), \tag{5}$$

where the zero in energy is taken to be the zero-point energy of HOONO, and C is chosen so that the maximum value of $I_{\mathrm{ABS}v'',n'';v',n'}(\nu,T)$ at 300 K is 100.

The above expression gives the absorption intensity for a specific $(v',n')\leftarrow(v'',n'')$ transition. Since the photodissociation product OH is detected in the action spectroscopy experiments, the detection efficiency depends on the quantum yield for dissociation. The dissociation threshold for *cis-cis* HOONO lies 490 cm^{-1} above the $2\nu_{\mathrm{OH}}$ overtone band. Therefore, based on harmonic frequencies, the overtone and combination bands involving one quantum of either of the two lowest frequency modes will not have enough energy to dissociate. As such, the intensity of each transition in the OH overtone absorption spectrum was multiplied by the fraction of the population at temperature T that has at least 490 cm^{-1} of vibrational excitation in other modes. This fraction is the estimated quantum yield for photodissociation, $\Phi_{n'}(T)$, which was multiplied by the absorption intensity to determine the action spectrum line intensities,

$$I_{\mathrm{ACTION};n'',v'',n'v'}(\nu,T) = \Phi_{n'}(T) \times I_{\mathrm{ABS};n''v'',n'v'}(\nu,T). \tag{6}$$

III. EXPERIMENT

Cavity ringdown spectroscopy (CRDS) was employed to experimentally obtain the direct absorption spectrum of *cis-cis* HOONO in the overtone region. HOONO was generated in a flow tube reactor at 20–40 Torr, with a gas mixture of 100 SCCM 1% H_2/He mix (SCCM denotes cubic centimeter per minute at STP) and 100 SCCM Ar flowing through a microwave discharge, combining with 200 SCCM 4% NO_2/N_2 (similar to the flow conditions for generating HOONO used in Bean *et al.*[2] and Fry *et al.*[6]). A purge flow of 200 SCCM dry N_2 per mirror was used to prevent destruction of the mirror surfaces. These flows result in a total composition in the cell of 0.125% H_2 and 1.0% NO_2 in bath N_2, Ar, and He.

At these concentrations, the primary reactions were

$$H + NO_2 \rightarrow OH + NO, \tag{7}$$

$$OH + NO_2 + M \rightarrow HONO_2 + M, \tag{1a}$$

$$OH + NO_2 + M \rightarrow HOONO + M, \tag{1b}$$

but a key side reaction was

$$OH + NO + M \rightarrow HONO + M. \tag{8}$$

Reference spectra of the two main interfering species, HONO and $HONO_2$, were recorded for spectral subtraction. Both species were generated by bubbling N_2 flow through liquid samples and flowing through the CRDS cell at 40 Torr. The HONO sample was generated by reaction of H_2SO_4 with $NaNO_2$ salt in aqueous solution, and the $HONO_2$ sample was 70% in H_2O, used as purchased from Aldrich.

Spectra were recorded by flowing the relevant gas mixture (discharge products or reference gas) through the center 50 cm long section of a cavity ringdown cell 2 cm in diameter. The optical cavity comprised two highly reflective mirrors (Nova Wave, R=99.995% centered at 1.5 μm) positioned on either end of the cell, spaced 82 cm apart. The mirrors were separated from the central flow region by 16 cm long purge volumes. Resulting empty-cell ringdown times were on the order of 10 μs.

The near-infrared (NIR) radiation, tunable through the range 6000–7000 cm^{-1}, was generated as the idler beam of a optical parametric oscillator (OPO) pumped by a 100 Hz tripled Nd:YAG (355 nm) (YAG—yttrium aluminium garnet) laser. Typical NIR pulse energies were 20 mJ with a laser linewidth of 4 cm^{-1}. Ringdown traces were accumulated with a GaGe Compuscope board (14-bit digitizer).

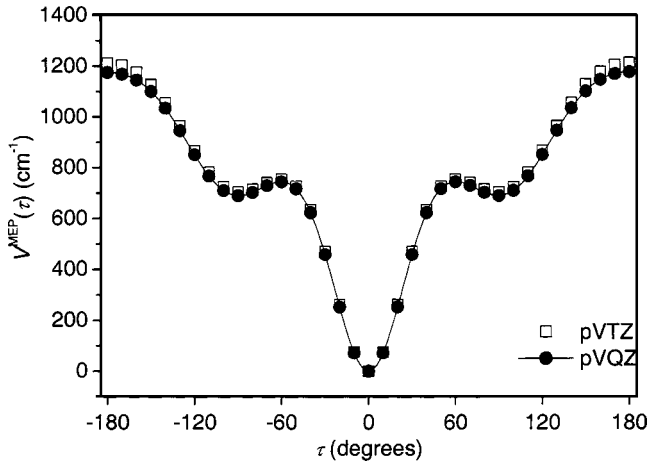

FIG. 2. Calculated torsional minimum energy potential (MEP), as a function of τ with the OONO dihedral angle constrained to 0°. Both potentials were calculated at the CCSD(T) level of theory using the cc-pVTZ (□) and cc-pVQZ (●) basis sets.

Traces from 40 laser shots were averaged before fitting. The averaged traces were fit to exponential functions using the Levenberg–Marquardt algorithm and averaged at each wavelength as the OPO was scanned through the range at a step size of 2 or 4 cm^{-1}. Scans of the full range were repeated in both scanning directions and at various step sizes to ensure that the relative intensities of the peaks were not influenced by slow changes in product concentrations due to fluctuations in the microwave discharge. Absorption spectra were obtained by subtracting the empty-cell ringdown spectra to account for background losses due to the ringdown mirrors.

IV. RESULTS

A. *Ab initio* one-dimensional torsional potential

The CCSD(T)/cc-pVQZ and CCSD(T)/cc-pVTZ torsional minimum energy potential (MEP) functions, $V^{\mathrm{MEP}}_{\mathrm{pVTZ}}(\tau)$ and $V^{\mathrm{MEP}}_{\mathrm{pVQZ}}(\tau)$, are plotted in Fig. 2. The energies and optimized structures along τ are reported in Table I of the EPAPS supplemental material for this paper.[29] The potentials that were obtained at these two levels of theory are nearly identical, indicating that the calculation is well converged with respect to basis set. The present results represent the highest level of theory applied to this system to date. Using the cc-pVQZ basis, the barrier for hindered rotation is 14.1 kJ/mol (1180 cm^{-1}), and occurs at τ=180°, the *cis-trans* configuration of HOONO. Near the equilibrium geometry, the potential appears to be fairly harmonic, but there is a plateau in the potential that extends from 50° to 110° that is roughly 8.4 kJ/mol (700 cm^{-1}) above the global minimum. On this surface, there is a slight local minimum at 90°. The depth of this well is sensitive to both the level of theory and basis set. An extensive search for a true local minimum, varying all geometric parameters, was conducted at the CCSD(T)/cc-pVTZ level but failed to find a minimum.

This region of the torsion potential near τ=90° will be referred to as the *cis-perp* configuration of HOONO. The shape of the torsional potential near this geometry also depends on the OH distance r, which was optimized in this calculation, and it is likely that it depends on the OONO torsion angle, which was fixed at 0° in these calculations. As such, we do not ascribe too much significance to the predicted depth (or lack) of the well, although, as we will see, the plateau has important implications for the spectroscopy.

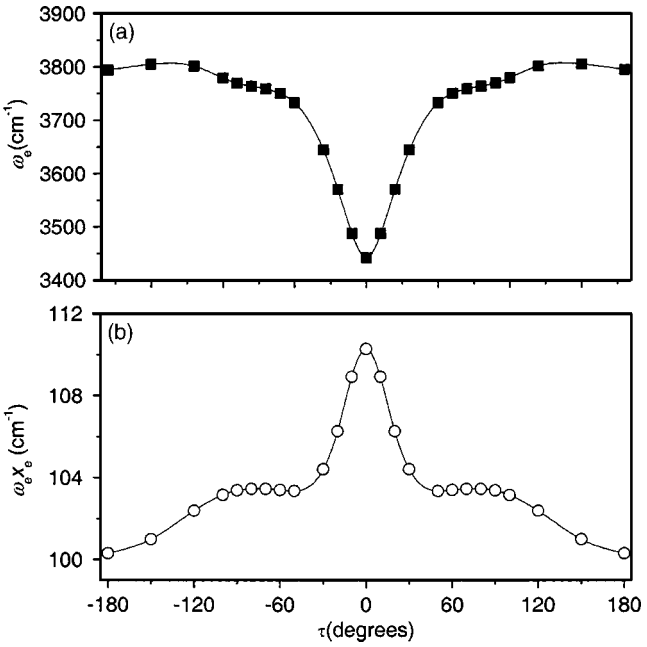

FIG. 3. (a) Harmonic frequency, $\omega_e(\tau)$, and (b) anharmonicity, $\omega_e x_e(\tau)$ for the OH stretch in *cis-cis* HOONO, derived from the parameters in the Morse fits of $U(r,t)$ in Eq. (3), plotted as a function of torsional angle τ.

B. Two-dimensional potential energy surface $U(r,\tau)$ and dipole moment surfaces $\mu(r,\tau)$

The two-dimensional potential energy surface $U(r,\tau)$ was evaluated over the range $r_e(\tau)-0.3$ Å$\leqslant r \leqslant r_e(\tau)+0.3$ Å and $0° \leqslant \tau \leqslant 180°$ by fitting the calculated CCSD(T)/cc-pVTZ points, and introducing scaling factors $\sigma(\tau)$ to correct for differences between the energies calculated using the cc-pVTZ and cc-pVQZ basis sets. This energy surface as a function of τ and r is reported in Table II of the EPAPS supplemental material for this paper.[29] The quality of the fit was tested by comparing the values of $r_e(\tau)$ and $U_e(\tau)$ to the values obtained from electronic structure theory. In all cases, $U_e(\tau)$ is within 12 cm^{-1} of $V^{\mathrm{MEP}}_{\mathrm{pVTZ}}(\tau)$, or better than 1%. The values of $r_e(\tau)$ agree to better than 0.05% or 0.0005 Å.

The harmonic frequencies $\omega_e^{(s)}(\tau)$ and anharmonicities $\omega_e x_e^{(s)}(\tau)$ for the one-dimensional OH vibration determined from the scaled Morse fits are plotted as a function of τ in Fig. 3 (Morse parameters are reported in Table III of the EPAPS supplemental material for this paper.[29]) Here we use the superscript (s) to indicate that they were calculated using the scaled surface. These quantities depend strongly on the HOON torsional angle, and change most rapidly at small angles. As τ is increased from 0° to 50°, the harmonic OH stretch frequency increases by 300 cm^{-1}, while the anharmonicity decreases sharply. This is consistent with an intramolecular hydrogen-bonding interaction between the OH group and the terminal O atom in the planar *cis-cis* configuration. Such a hydrogen bond softens the OH bond and makes it

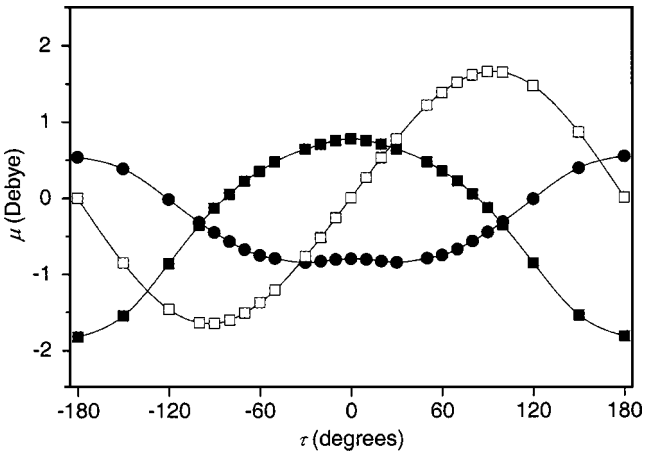

FIG. 4. One-dimensional slices of the dipole moment surface $\mu(r,\tau)$ evaluated at equilibrium OH bond lengths, $r_e(\tau)$, projected onto the three principle axes, defined in the text. μ_A (■), μ_B (●), and μ_C (□). Surface computed at QCISD/AUG-cc-pVTZ level.

more anharmonic, but it is very directional and its effect on the OH vibration weakens quickly as τ is changed.

The two-dimensional surfaces for the three components of the dipole moment were determined at the QCISD/AUG-cc-pVTZ level, at the same values of r and τ that were used to obtain the two-dimensional potential surface. In order to estimate the effects of the size of the basis set on the computed value of the dipole moment, the dipole moment was reevaluated at a subset of the configurations (three values of r at $\tau=0°$, 20°, and 60°) at the QCISD/AUG-cc-pVDZ level. For these points, the dipole moment values computed with the two basis sets differed by less than 3%.

The values of the dipole components along the minimum energy path ($r=r_e(\tau)$) are plotted as a function of r in Fig. 4, and the values of all of the calculated points on the three components of the dipole surface are reported in Tables IV–VI of the EPAPS supplemental material for this paper.[29] The two in-plane components (A and B) are symmetric with respect to τ and are relatively flat over the range $-50°<\tau<50°$. However, the C (out-of-plane) component has a strong dependence on τ, and is of odd symmetry. The first derivative of this component of the dipole is 0.0258 D/deg at 0°. The differences in the properties of the three components of the dipole moment are consistent with $\Delta n=\pm 1$ transitions carrying significant intensity and having C-type band contours, whereas the $\Delta n=0$ transitions will have A- and/or B-type band contours. The slices through the dipole moment surface as a function of r for a given τ are fit to a cubic polynomial, centered at $r_e(\tau)$. The raw data and resulting parameters are reported in Tables IV–VII of the EPAPS supplemental material for this paper.[29] Fits to lower and higher order polynomials were also performed and it was found that quadratic through quartic expansions of the dipole moment surface lead to spectra with intensities in near exact agreement.

C. Calculated vibrational energy levels, wave functions, and vibrationally adiabatic potentials

The vibrational energy levels $E(v,n)$ were obtained by solving the two-dimensional Hamiltonian, and are identified

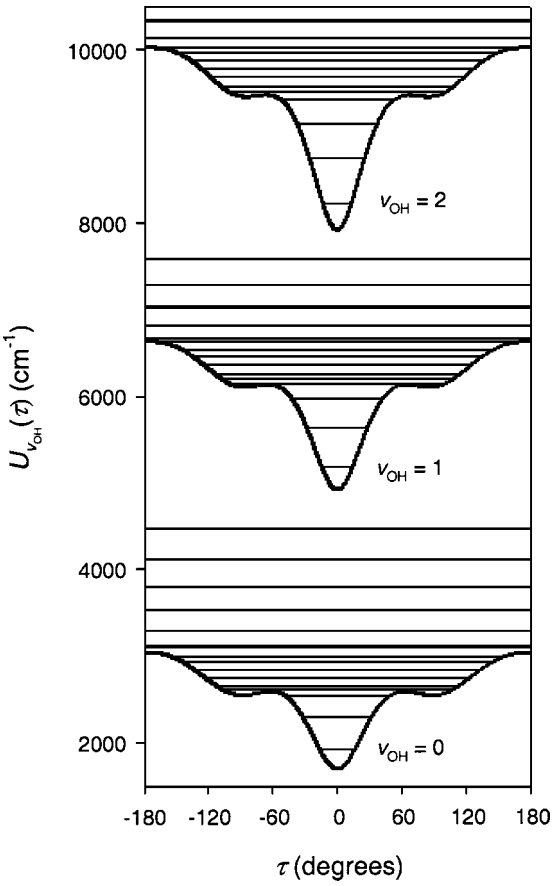

FIG. 5. Vibrationally adiabatic potential energy surfaces $U_{v_{OH}}$ for $v_{OH}=0$, 1, and 2, plotted as a function of τ. The thin lines on each of the adiabatic potential curves represent the energies $E(v_{OH},n)$ of the torsional states that are associated with the specific v_{OH} quantum level.

by the quantum numbers n for the HOON torsion mode and v for the OH stretch mode. The effect of torsion-stretch coupling is most clearly seen by plotting the vibrationally adiabatic torsion potentials $U_v(\tau)$, obtained by averaging the two-dimensional surface over a specific v state in the OH stretch. This is achieved by evaluating

$$U_v(\tau)=\omega_e^{(s)}(\tau)\left(v+\frac{1}{2}\right)-\omega_e x_e^{(s)}(\tau)\left(v+\frac{1}{2}\right)+U_e^{(s)}(\tau), \quad (9)$$

where the harmonic frequency and anharmonicity are obtained from the scaled potential $U(r,\tau)$, using the standard relationships. These potentials are shown in Fig. 5. In contrast to $V^{\mathrm{MEP}}(\tau)$, which is the bare electronic energy computed along the minimum energy path, $U_v(\tau)$ is the one-dimensional effective potential which includes the vibrational energy of the vth OH stretch state.

As illustrated in Fig. 5, the shape and depth of the adiabatic torsional potentials depend on the amount of OH-stretch excitation. The τ dependence of $\omega_e^{(s)}$ and $\omega_e x_e^{(s)}$, plotted in Fig. 3, illustrates that the OH vibrational energy in Eq. (9) increases sharply with τ. Consequently, the vibrationally adiabatic torsional potentials are deeper than $V_{\mathrm{pVQZ}}^{\mathrm{MEP}}(\tau)$, plotted in Fig. 2, and they become deeper with increasing v.

The first-order effect of the OH-stretch torsion coupling is to increase the barrier height of the hindered rotation, i.e., the energy of *cis-trans* HOONO. The barrier on the scaled

surface increases from 1342 to 1715 cm^{-1} and 2107 cm^{-1} in the $v=0$, 1, and 2 potentials, respectively. This can be compared to the barrier of 1175 cm^{-1} in $V_{pVQZ}^{MEP}(\tau)$. Much of the vibrational dependence of $U_v(\tau)$ is seen at small angles, and the curvature of the torsion potential at the *cis-cis* HOONO minimum is found to increase with increasing OH stretch excitation. This leads to an increase in the difference between the energies of the states with $n=0$ to $n=1$ from 380 cm^{-1} when $v=0$, to 462 cm^{-1} and 537 cm^{-1} when $v=1$ and 2, respectively. Finally, the *cis-perp* HOONO minimum in the one-dimensional surface becomes shallower with increasing OH excitation. The value of the potential in the *cis-perp* configuration ($\tau=90°$), measured relative to the *cis-cis* HOONO minimum, e.g., $U_v(90°)-U_v(0°)$, increases from 848 cm^{-1} for $v=0$ to 1190 cm^{-1} for $v=1$ and 1545 cm^{-1} for $v=2$. This can be compared to the value of the potential along the minimum energy path at the *cis-perp* geometry, where $V_{pVQZ}^{MEP}(90°)=690$ cm^{-1}. The dramatic changes in the torsional potential and frequencies with OH-stretch excitation reflect the large decrease in the OH-stretch frequency in the hydrogen-bonded *cis-cis* configuration.

On each of the one-dimensional adiabatic surfaces, $U_v(\tau)$, in Fig. 5, we plotted the energy of the associated two-dimensional vibrational states. Since we are solving the Schrödinger equation for a two-dimensional system for $v>0$, there will be states with multiple values of v in a given energy range. As such, for a given v, we only showed the energies of, at most, the 20 lowest energy states for which

$$P_v^m = \int_0^{2\pi} d\tau |\langle \psi_v(r)|\Psi_m(r,\tau)\rangle|^2 > 0.75. \tag{10}$$

Here $\psi_v(r)$ represents an eigenstate of the one-dimensional stretch problem, obtained from the one-dimensional slice through our two-dimensional surface at $\tau=0$, while $\Psi_m(r,\tau)$ is a solution to the two-dimensional stretch-torsion Hamiltonian, described above. For these states, we replace the general index *m* by the combined index v and n, where the value of n is determined by the number of zeros in the integrand.

For $v=0$, the states with $n=0$, 1 and 2 lie below the barrier that separates the *cis-cis* and *cis-perp* HOONO minima and are confined to the *cis-cis* well on the $U_0(\tau)$ adiabatic surface. The highest of these states lies 848 cm^{-1} above the minimum of the $U_0(\tau)$ adiabatic surface and less than 1 cm^{-1} below the *cis-perp* minimum on this surface. There are six additional states that have energies that are at or below the *cis-trans* barrier to free rotation of the OH about the OO bond. In addition, we note that the density of states increases sharply just above the *cis-perp* shelf, because the well opens up rather abruptly at 50°. At energies above the *cis-trans* barrier, the level spacings begin to increase and the states become doubly degenerate as they approach the n^2 dependence of a one-dimensional free rotor. When the OH bond is excited to the $v=1$ or 2 states, the *cis-cis* well deepens and narrows, while the plateau about the *cis-perp* conformer and the *cis-trans* barrier height increase. As a result, for $v=2$, four states have energies below the *cis-perp* shelf, and these states have larger level spacings than those with $v=0$.

In Fig. 6 we plot the projections of the probability densities onto τ for the six lowest energy states ($v=0$) depicted by horizontal lines in $U_0(\tau)$ of Fig. 5. The first four of these states can be best described as a progression of states in the *cis-cis* well with $n=0$–3. There is a sharp increase in the range of the potential sampled by these states and the states with $n>3$. In fact, the $n=4$ state has most of its probability amplitude in the region $45°<|\tau|<120°$ and can be best described as having an anomalously large probability in the *cis-perp* region of the potential. This apparent localization results from the fact that as the potential well opens up near $\tau=90°$, the zero-order description of this motion, e.g., small vibrations about the *cis-cis* HOONO minimum, is no longer valid. As a result of this rapid increase in the range of motion along τ we find that there are two states that are close in energy, one of which is the next state in the progression of vibrational levels from the *cis-cis* HOONO minimum and another which has greater probability amplitude near the *cis-perp* shelf. This is seen in spite of the fact that the well at the *cis-perp* HOONO configuration is quite shallow. While we have not plotted the states for other values of v, the general trends are the same, and the wave functions that correspond to the horizontal lines in Fig. 5 retain their clean nodal structure. The states that have energies lower than the *cis-perp* shelf are localized in regions where $|\tau|<60°$, while the states just above the shelf have anomalously large probability amplitude in the *cis-perp* region of the potential.

D. Calculated absorption and action spectra

Our calculated spectra are shown in Fig. 7. The spectra were generated using the two-dimensional model described above, with a temperature of 300 K. In each of the plots we present a stick spectrum as well as the results a convolution of the stick spectrum by a Gaussian with a full width, half maximum of 70 cm^{-1}, which is chosen to reproduce the observed experimental broadening. In Table I we list some of the most important $(n',v'=2)\leftarrow(n'',v''=0)$ overtone transitions, along with their respective transition frequencies, transition strengths, absorption intensities, and action intensities, as defined in Eqs. (4)–(6).

1. Absorption spectra

The calculated absorption spectra for the fundamental and overtone at 300 K are shown in Figs. 7(a) and 7(b). In both spectral regions, the dominant peak is the origin, and only one transition, the $n=0\leftarrow 0$ band, contributes to its intensity. All of the other bands with significant intensity—combination bands, sequence bands, and hot bands—are shifted to the blue of the origin by 100–600 cm^{-1}. In the convoluted spectra, there is one very broad satellite band in the fundamental region and four narrower satellite bands for the first overtone.

The overtone absorption spectrum is most relevant to the current study. The first two smaller bands adjacent to the $2\nu_{OH}$ origin, **B** and **C**, are approximately 10% and 2% of the intensity of the origin. Each has a single dominant contribution, from $n=1\leftarrow 1$ and $n=2\leftarrow 2$ transitions, respectively. Thus, these levels are "Franck–Condon-like" $\Delta n=0$ se-

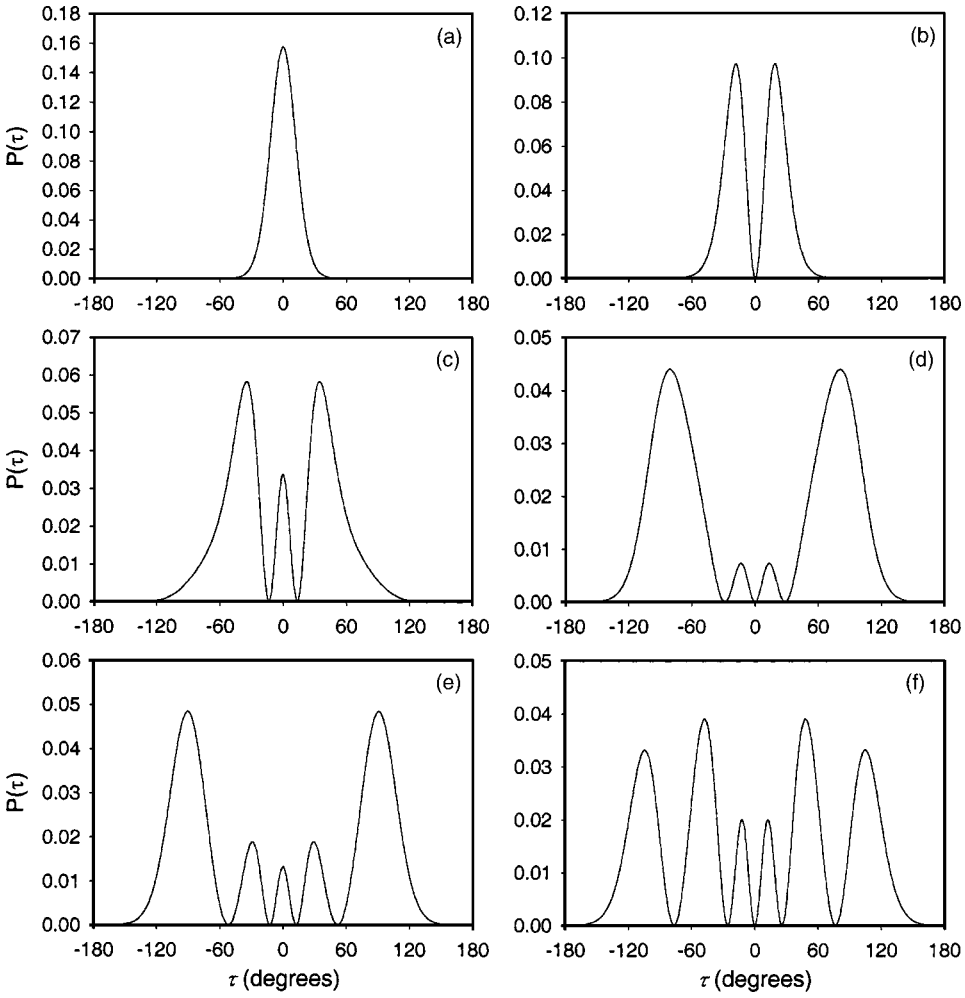

FIG. 6. Probability densities for the six lowest energy states ($v_{OH}=0$, $n=0$–5), projected onto τ.

quence bands. Such large shifts in the sequence band frequencies are a direct result of the stretch-torsion coupling, which leads to the increased energy level spacing of the torsion states in $U_2(\tau)$ versus $U_0(\tau)$, discussed above. These bands are comparable in transition strength to the origin, but appear weak due to their low populations.

The two higher energy bands in the overtone spectrum are pileup bands of several transitions. The third band **D** is ~10% the intensity of the origin. We assign this band to a series of largely unresolved $\Delta n=+1$ *C*-type transitions. The $n=4\leftarrow 3$ transition is the strongest single line, although the transitions with $n''<6$ all carry intensities that are within a factor of 4 of this transition. As such, the main contribution to the overall intensity of the convoluted band comes from the sum of the intensities of transitions with $n''=0$ through 6. As we noted above, the states with $n''\geqslant 3$ have energies above the *cis-perp* plateau, and thus many of the transitions in this band arise from states with significant probability amplitude in the *cis-perp* HOONO geometry. As seen in Table I, the individual $\Delta n=+1$ transitions have large transition strengths for $n''\geqslant 2$, a reflection of the fact that the intensity in this band comes from the *C* component of the dipole vector (e.g., the component that is perpendicular to the OONO plane). It is interesting to note that the states with $n''\geqslant 2$ are at least 628 cm^{-1} higher in energy than the vibrationless level, so that they are expected to be weak based on the Boltzmann factor. However, this decrease in population is compensated by the factor of 50 increase of the transition strength for the $n=4\leftarrow 3$ transition, compared to $1\leftarrow 0$ transition. A fourth weak band, labeled **E**, is another pileup of weak bands with a significant contribution from $\Delta n=+2$ transitions, which appear as a single peak after convolution.

The ν_{OH} fundamental region of the absorption spectrum is similar to the overtone region, although the magnitudes of the blueshifts are less, as expected. Only one satellite band, located 333 cm^{-1} to the blue of the origin, has appreciable intensity (15% of the origin). It arises from the series of $\Delta n=1$ transitions, described above. The $n''=1\leftarrow 1$ and $n''=2\leftarrow 2$ are seen in the stick spectrum with 10% and 2% of the intensity of the most intense transition, the smaller blueshift of these bands leads them to be incorporated as a blue shoulder in the envelope of the most intense transition.

The overtone absorption spectrum at 233 K is shown as a dotted line in Fig. 7(b). The two curves are normalized such that the origin peaks 6310 cm^{-1} have the same intensity. At the lower temperature, the sequence bands and hot bands are approximately three times weaker, due to the lower the Boltzmann factor $f_{v'',n''}(T)$ of the torsionally excited levels.

2. Action spectrum

The primary difference between the absorption and action spectra arises from the fact that the action spectrum

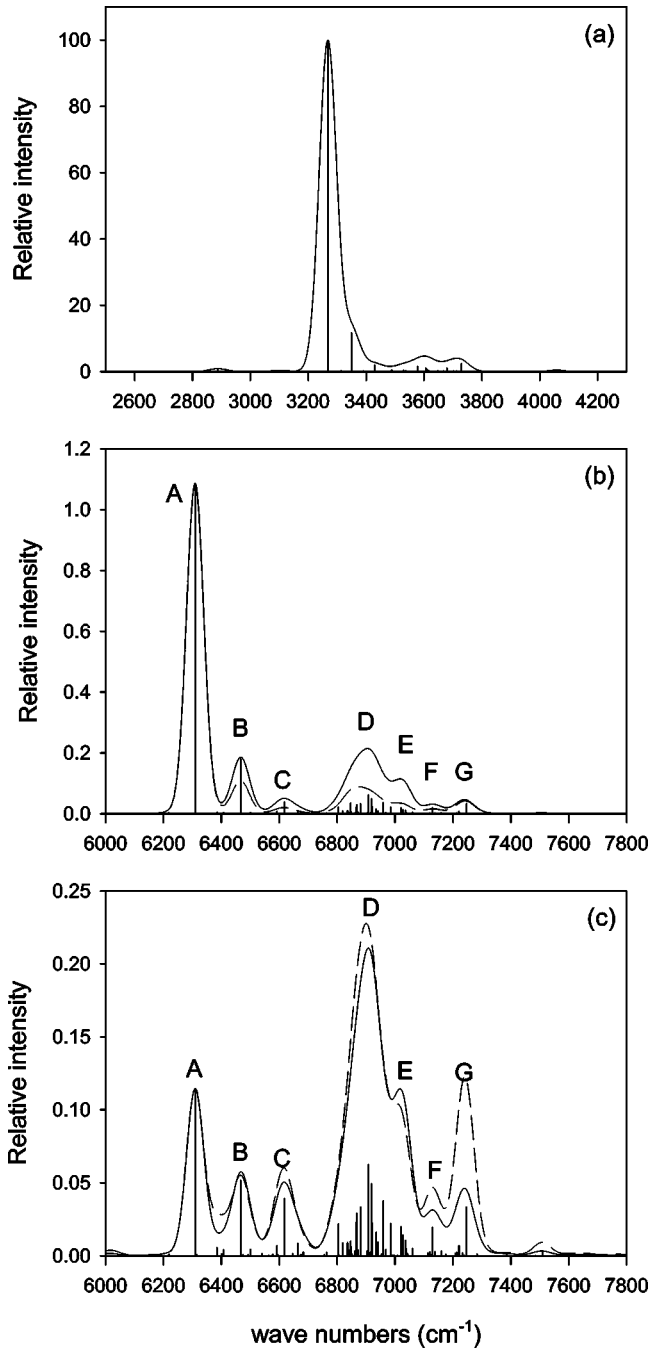

FIG. 7. Spectra, calculated at 300 K (solid) and 233 K (dashed) for the fundamental (top), first overtone (middle), and the first overtone multiplied by the quantum yield for photodissociation given in Eq. (6) (bottom). In all three spectra, the stick spectrum is convoluted with a Gaussian with a full width half maximum of 70 cm^{-1} and all plots at 300 K are normalized so that the maximum value of the stick and convoluted spectra in (a) are 100, while the spectra at 233 K in (b) and (c) are normalized so that the peak maxima at ~6300 cm^{-1} have the same relative intensities.

requires that the excited HOONO dissociate to $OH+NO_2$. We expect that intramolecular vibrational-energy redistribution (IVR) and dissociation will be fast and assume that any excited state above D_0 will predissociate and contribute to the action spectrum. Thus, in our quantum yield calculation we count states that are prepared with energy above D_0.

Experimentally, the $2\nu_{OH}$ state lies 490 cm^{-1} below the dissociation threshold, based on the estimation of D_0(*cis-cis* HOONO) of Konen *et al.*[18] On the other hand, at 300 K hot bands are populated. Therefore, if we neglect off-diagonal anharmonicities between (r,τ) and the seven remaining vibrational modes, we can approximate the action spectrum by weighting the absorption intensity by the fraction of the vibrational partition function that reflects contributions to the intensities of transitions to states with at least 490 cm^{-1} of vibrational energy above the $2\nu_{OH}$ overtone.

The procedure for achieving this is described above. We use the harmonic frequencies obtained at the CCSD(T)/cc-pVTZ level of theory. When we analyzed the vectors associated with the two torsional modes, which had frequencies of 383 and 523 cm^{-1}, we found that they were highly mixed. In fact, when we performed the harmonic analysis making either the mass of hydrogen or the masses of the heavy atoms very large, thereby setting one of the torsion frequencies to zero, we found that the HOON torsion frequency became 439 cm^{-1}, while the OONO torsion frequency became 462 cm^{-1}. This indicated that there is large mixing of the two torsional modes at the harmonic level. As such, we use the average of the two torsion frequencies in place of the calculated OONO frequency. Operationally the above procedure requires us to scale transitions to the $2\nu_{OH}$ state by $\Phi_0(300\ K)=0.104$ and transitions to the combination band with 2 quanta in the OH stretch and one in the torsion by $\Phi_1(300\ K)=0.288$. At 233 K, we find that the quantum yields have decreased to $\Phi_0(233\ K)=0.0352$ and $\Phi_1(233\ K)=0.1566$.

The resulting stick and convoluted spectra $I_{ACTION}(\nu,T)$, taking into account the nonunity quantum yield $\Phi_{n'}(300\ K)$, is plotted in Fig. 7(c). Action spectrum intensities of specific transitions are listed in Table I.

Comparing the spectra in Figs. 7(b) and 7(c) reveals a dramatic change in the relative band intensities in the overtone spectrum upon inclusion of the quantum yield correction in Eq. (6). The first three bands, **A**, **B**, and **C**, are the same as observed in the absorption spectrum (the $n=0\leftarrow 0$, $n=1\leftarrow 1$, and $n=2\leftarrow 2$ transitions), but the origin is almost ten times weaker, only a factor of 2 to 3 stronger than the next two bands. The most prominent feature in the calculated action spectrum is now the large peak at 6900 cm^{-1} (**D**). This peak has roughly twice the peak intensity of the origin and is substantially broader, indicating that it accounts for more of the total band strength.

As in the absorption spectrum, the **D** band is composed of many transitions, the majority of which are $\Delta n=+1$ lines. This is a reflection of the fact that the intensity in this band comes from the *C* component of the dipole vector (e.g., the component that is perpendicular to the OONO plane). As is seen in Fig. 4, its value increases from zero in the planar configuration to 1.5 D in the *cis-perp* HOONO configuration. The most intense of these transitions originates from the $n''=3$ state, with significant contributions from states up to $n''=7$. This band is composed of hot bands primarily from states that sample the *cis-perp* HOONO geometry. Additional side bands to the blue of the 6900 cm^{-1} peak, labeled **E**, **F**, and **G**, arise from $\Delta n=+2$ transitions, originating from the ground state (**G**), the state with $n''=1$ (**F**), and a pileup of states with $n''>1$ (**E**).

TABLE I. Frequencies, relative absorption and action intensities at 300 K, and absolute transition strengths for the strongest transitions in the calculated *cis-cis* HOONO spectrum, discussed in the text.

n''	n'	ν(cm^{-1})	Band[a]	$I_{ABSv'',n'';v',n'}$[b]	$I_{ACTIONv'',n'';v',n'}$[b]	$I_{v'',n'';v',n'}$ (cm^{-1} D^2)
0	0	6309	**A**	1.000	0.104	0.3744
1	1	6467	**B**	0.166	0.048	0.3839
2	2	6617	**C**	0.036	0.036	0.2752
3	3	6804		0.020	0.020	0.2219
0	1	6847	**D**	0.032	0.009	0.0121
1	2	6866	**D**	0.021	0.021	0.0491
2	3	6881	**D**	0.031	0.031	0.2342
3	4	6907	**D**	0.058	0.058	0.6353
4	5	6918	**D**	0.043	0.043	0.6077
0	2	7246	**G**	0.031	0.031	0.0115

[a]As identified in Figs. 7(b) and 7(c).
[b]Defined in Eqs. (5) and (6). The values are normalized so that for the $0 \leftarrow 0$ transition in the absorption, the intensity is unity.

The overtone action spectrum at 233 K is shown as a dashed line in Fig. 7(c). We have again normalized the spectra so that the origin peaks at 6310 cm^{-1} have the same intensity. In the action spectrum case, in contrast to the absorption spectrum, there is strikingly little change in the relative band intensities with changing temperature.

E. Experimental results

The cavity ringdown absorption spectrum of products from the discharge reaction $H+NO_2$ is shown in Fig. 8(a). The spectrum was recorded at 300 K and a total pressure of 40 Torr; the background empty-cell ringdown spectrum has been subtracted. The ordinate is the absorption in units of ppm per pass in the cavity ringdown cell (where the effective pass length is estimated to be about 50 cm). No attempt was made to measure an exact absorption cross section.

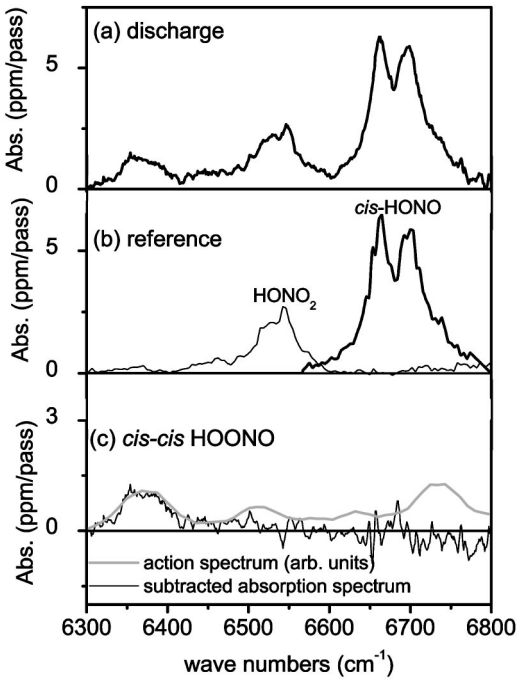

FIG. 8. Direct absorption spectrum of *cis-cis* HOONO recorded by cavity ringdown of $OH+NO_2$ system, reaction path length $L \approx 50$ cm. (a) Spectrum of products formed in the discharge reaction. (b) Reference spectra of HONO and HNO_3 and scaled to match intensities in (a). (c) Spectrum of *cis-cis* HOONO obtained by subtracting reference spectra from discharge spectrum (curve), compared to the smoothed action spectrum of *cis-cis* HOONO (Ref. 6) in the same spectral region.

Reference spectra of HONO (centered at 6680 cm^{-1}, assigned as the $2\nu_1$ band of *cis*-HONO by Guilmot *et al.*[30]) and $HONO_2$ (centered at 6530 cm^{-1}, assigned as the $2\nu_1-\nu_9$ band by Feierabend *et al.*[31]) are shown in Fig. 8(b). Above 6850 cm^{-1}, the $HONO_2$ $2\nu_1$ band dominates, and no subtraction is possible. The spectra have been scaled in intensity to best fit matching bands in the discharge spectrum.

The subtracted cavity ringdown spectrum, 6300–6800 cm^{-1}, is shown in Fig. 8(c); only one feature remains after subtraction of HONO and $HONO_2$, a band at 6370 cm^{-1}. The subtracted spectrum to the blue of this band, from 6400 to 6800 cm^{-1}, is noisier, primarily due to difficulties with background subtraction and to mirror reflectivity. No additional bands are evident in the absorption spectrum in this region; any absorption bands must have intensities on the order of 10% or less of the origin band. No additional absorption was observed up to 6850 cm^{-1}.

The band at 6370 cm^{-1} is roughly 30–50% of the intensity of the *cis*-HONO band, a result similar to previous observations of *cis-cis* HOONO and *cis*-HONO band intensities in the fundamental region.[2] As this is the only peak observed and has reasonable intensity, we assign this band to the origin of the *cis-cis* HOONO $2\nu_{OH}$ spectrum. This peak has no resolvable structure but has a slightly asymmetric flat-top profile that does not match either Gaussian or Lorentzian line shapes. The bandwidth, 60 cm^{-1} (FWHM), is approximately 50% wider than predicted by a rotational contour simulation for this band.[6]

V. COMPARISON OF CALCULATED AND EXPERIMENTAL SPECTRA

The two-dimensional calculations of the first overtone spectrum of *cis-cis* HOONO predict that the intensity pattern in the action spectrum will differ significantly from the absorption spectrum, due to quantum yield effects. By detect-

ing the CRDS spectrum of this region, we are now in a position to test this prediction and to evaluate the extent to which the coupling of just two modes, the OH stretch and HOON torsion, can account for the previously observed action spectrum.

To compare experimental and calculated spectra, we must shift the absolute frequency scale of the calculated absorption and action spectra by 55 cm^{-1} in order to match the origin in the calculated spectrum with the 6365 cm^{-1} (6370 cm^{-1}) peaks seen in the experimental action (absorption) spectra. Such a shift is well within the uncertainties of the *ab initio* calculation as well as uncertainties stemming from neglect of vibrational couplings with the seven other modes.

In the case of the action spectrum, the strongest feature in the experimental spectrum is the broad band 600 cm^{-1} to the blue of the origin. A band at a similar shift and with large relative intensity (**D**) is also seen in the calculated spectrum. Examining the stick spectrum that underlies this feature, we find that this band has contributions from a series of overlapping $\Delta n = +1$ hot band transitions from torsionally excited molecules. The most intense of these originates from the $n'' = 3$ state. Transitions originating from states with $n'' \leqslant 7$ carry intensities that are at least 15% of the intensity of the most intense band in this progression.

There are two additional features to the blue of the large 6970 cm^{-1} peak in the experimental action spectrum, at 7130 and 7240 cm^{-1}. Similar bands to the blue of the large band are seen in the calculated spectrum (**F** and **G**) and arise from $\Delta n = +2$ transitions from the states with $n'' = 1$ and 0, respectively. The intensity of the **G** band was observed by Fry *et al.*[6] to increase slightly with decreasing temperature, in agreement with the change seen in the calculated spectra from 300 to 233 K. The remaining features that are seen in both the observed and calculated action spectra are the peaks at 6500 and 6640 cm^{-1}. These are assigned to the $n = 1 \leftarrow 1$ (**B**) and $n = 2 \leftarrow 2$ (**C**) sequence bands, respectively.

While many of the peaks in the experimental spectrum are reproduced in the calculated spectrum, there are experimental features that are not found in the calculation. Of the major bands, only the band at 6730 cm^{-1} in Fig. 1 is not reproduced by these reduced dimensional calculations. This band is most likely a combination or sequence band involving one of the seven vibrational modes that are not included in this model. Based on the position of this band and the harmonic frequencies of *cis-cis* HOONO, this band is most likely a combination band that involves another mode.

In contrast to the action spectrum, the calculated absorption spectrum consists of a single strong band at the origin, with the other bands possessing intensities $<5\%$ of the origin. The experimental CRDS absorption spectrum, shown in Fig. 8(c), confirms these predictions, up to 6850 cm^{-1}. In Fig. 8(c), the experimental CRDS absorption spectrum is compared to the previously reported action spectrum. As expected, the absorption spectrum has only one strong band, at 6370 cm^{-1}. This band is nearly identical to the band (**A**) in the action spectrum at essentially the same frequency and is assigned as the origin. None of the features present in the action spectrum at 6505, 6640, or 6730 cm^{-1} are seen in the direct absorption spectrum, within our signal-to-noise. Thus, the intensity patterns of the experimental action and absorption spectra differ qualitatively, in accord with our predictions.

Unfortunately, background absorption by the $2\nu_{OH}$ band of nitric acid at 6944 cm^{-1} overwhelms any signal above 6850 cm^{-1} and prevents us from detecting any HOONO absorption. Consequently, we cannot rule out the presence of the strong 6970 cm^{-1} band seen in the action spectrum. Thus, complete verification by experiment of the effects of quantum yield on the overtone spectrum must await experiments that can observe this band directly.

VI. DISCUSSION

A. Limitations of calculated spectra

Our two-dimensional model captures much of the essential physics of this system through consideration of only the coupling between the HOON torsion and the OH-stretch motions; however, like any reduced dimensional model, it has limitations. Specifically, we know that HOONO has nine degrees of freedom, three of which have relatively low frequencies. Further, just as motion in the HOON torsion will break the intramolecular hydrogen bond in the equilibrium configuration, so will motion along the heavy atom torsion and the in-plane breathing mode. Our calculations indicate that the two torsional modes have the same symmetry and nearly identical frequencies. The lowest torsional levels are thus likely to be highly mixed.

We expect that there will also be significant anharmonic couplings between the OH-stretch vibration and the other two low-frequency vibrational modes. Furthermore, Fermi resonances between the OH stretch and the OOH bend are often evident in overtone spectra. As a result, there are features in the spectrum that cannot be accounted for in this model. We note that parallel to these studies Stanton and co-workers[13] have been using perturbation theory to calculate frequencies and intensities of transitions in the $2\nu_{OH}$ region in the spectrum. The 6730 cm^{-1} band that is not assigned using this two-dimensional model appears to be accounted for as a different combination band in their model.

In addition to missing seven vibrational degrees of freedom, the calculated relative intensities of the action spectrum are also very sensitive to the choice of D_0. The experiment of Konen *et al.*[18] pinpoints D_0 with high precision, but since the dissociation limit falls in the middle of the overtone spectrum, even small shifts in D_0 or in the predicted vibrational frequencies will alter the calculated intensity patterns. Our treatment of the quantum yield is also simple; we consider only which vibrational levels are above or below dissociation. We neglect effects due to dissociation lifetimes and collisional relaxation or excitation, processes which lead to pressure dependent quantum yields that may be important very close to threshold. Finally, we neglect rotations, which couple to the torsion, but also can lead to centrifugal barriers and hence influence dissociation yields.

In spite of the above comments it is quite remarkable how well a two-dimensional model based entirely on *ab initio* energies and frequencies, with the dissociation en-

ergy as the only experimentally constrained parameter, reproduces nearly all of the major features in the recorded action spectrum.

B. Interpretation of the action spectrum

This work clarifies the physical basis for the experimentally observed first overtone action spectrum of *cis-cis* HOONO.[1,6] We find that most of the peaks in the observed action spectrum (Fig. 1) are hot bands, i.e., are transitions from initial states that are vibrationally excited. The first three prominent peaks are $\Delta n=0$ sequence bands. Of these, the $n=0\leftarrow 0$ and $n=1\leftarrow 1$ must arise from hot *cis-cis* HOONO molecules with vibrational excitation in modes other than the OH stretch or the HOON torsion, in order to result in a final state that is above the dissociation threshold. While the photon energy of the broad **D** band exceeds the dissociation energy of 6860 cm^{-1}, this band is also composed of transitions from torsionally excited molecules, primarily $\Delta n=+1$ from higher n'' states.

In previous work, the strength of the 6970 cm^{-1} band was puzzling. We find that several effects contribute to the intensity of this band. First, the intensity of this band does not result from borrowing intensity from the zeroth order $2\nu_{OH}$ state, as is often seen in overtone spectra, e.g., in Fermi resonance states. This is evidenced by the clean nodal patterns in the vibrational wave functions associated with the states that are indicated by the horizontal lines in Fig. 5. As is seen in Table I, the $\Delta n=+1$ transitions from higher level torsional states, e.g., $n=4\leftarrow 3$ and $n=5\leftarrow 4$ actually have larger transition strengths than the origin band. The origin of this enhancement is due in part to the large derivative of the C component of dipole moment with τ. In addition, comparing the states on the adiabatic surfaces with zero and two quanta in the OH stretch, plotted in Fig. 5, we find that the states that are just above the *cis-perp* shelf differ in the number of quanta in the torsion by one. This reflects the deepening of the *cis-cis* well with increasing OH-stretch excitation. This leads to an increase in the magnitude of the matrix elements of the dipole moment operator, and from that the intensities of these $\Delta n=+1$ transitions. Second, there is an unusually high density of states starting at $n''=2$, which stems from the opening of the potential at the *cis-perp* shelf. Thus, while we do not find any states that are truly bound in a *cis-perp* well, the probability density of the states just above this shelf indicates that the vibrationally averaged structure of these molecules is effectively the *cis-perp* geometry. These are the states that predominantly contribute to the **D** band.

The current results also resolve a puzzling discrepancy. Fry *et al.*[6] observed no change in the major features in the experimental action spectrum as they lowered the temperature. However, they expected that bands with photon energies below the dissociation limit D_0 would appear weaker at lower temperatures. Using statistical RRKM calculations, they predicted that the quantum yield would fall off rapidly for $h\nu<D_0$. The origin band intensity was estimated to decrease by over a factor of 2 relative to the **D** band, which lies above D_0.

As seen in Fig. 7(c), the calculated action spectra at 233 K and 300 K show no significant change in relative band intensities with decreasing temperature, demonstrating that the value of $D_0=6860$ cm^{-1} obtained by Konen *et al.*[18] is consistent with the results of Fry *et al.*[6] The surprising similarity of the two plots in Fig. 7(c) can be explained by the observation that the action spectrum is largely due to hot bands of *cis-cis* HOONO. As the temperature is reduced from 300 to 233 K, transitions originating out of the more populous states, $n''=0$ or 1, have smaller quantum yields, while transitions originating out of higher energy torsionally excited states $n''>1$, decrease in intensity as their populations decrease. The reductions in quantum yields for the lower frequency $n''=0$ or 1 transitions nearly exactly match the decrease in the higher frequency bands excited from torsionally hot states. Thus, the overall intensity of the action spectrum decreases almost identically across all bands, and the relative intensities of most of the bands remain unchanged.

There are two notable exceptions to the consistency in band intensity ratios with changing temperature. The **F** and **G** bands in the calculated spectrum are predicted to increase in intensity when the temperature is decreased from 300 to 233 K. The increase in the intensity of these transitions in the calculated spectrum reflect the fact that they are assigned to the $\Delta n=+2$ transition from the $v=1$ and 0 levels and are transitions that have unit quantum yield for dissociation, within our model. The experimental data support this, as the band at 7230 cm^{-1} in the experimental action spectrum also increased in intensity with decreasing temperature from 273 to 193 K.[6] The unassigned band in the experimental action spectrum also showed an increase in intensity with decreasing temperature, consistent with its assignment as a band from the ground state to a combination level of $2\nu_{OH}$ with excitation in at least one of the seven vibrations not included in the present model.

C. Implications for the HOONO yield in the $OH+NO_2$ reaction

Bean *et al.* determined the $HOONO/HONO_2$ yield in reaction (1) by measuring the integrated band intensities of the respective fundamental modes, and converting these to densities using the ratio of CCSD(T)/AUG-cc-pVTZ cross sections computed in the double harmonic approximation for *cis-cis* HOONO.[2] Thus, they made the assumption that all molecules of both species were absorbing in the ν_{OH} band. This is in fact true for $HONO_2$ (the main sequence band is within the envelope of the fundamental). However, the current calculations [Fig. 7(a)] demonstrate that the strong stretch-torsion coupling shifts all of the HOON torsional hot bands (sequence or otherwise) more than 80 cm^{-1} away from the origin of the fundamental band. Thus, integration of the absorption at the origin band excludes states with $n''\geqslant 1$. Based on the harmonic oscillator partition function, the measurement given by Bean *et al.* must underestimate the *cis-cis* HOONO population by $\approx$20%.

These considerations lead us to the tentative conclusion that the low pressure $HOONO/HONO_2$ branching ratio

should be significantly higher than the 7.5% measured by Bean *et al.*[2] (300 K and 13 Torr). To quantify fully this effect, more accurate integrated intensities, taking into account anharmonicity of the OH stretch, must be computed for both HOONO and $HONO_2$. Furthermore, all of the other modes must be included. Coupling with other modes, notably the low-frequency bending/breathing mode ν_7 and OONO torsion ν_8 will alter the frequency shifts. However, if these modes also lead to large shifts in their respective hot bands, then the ratio could be even larger.

D. Mechanism for broadening of the overtone spectrum

The current results shed additional light on the spectral broadening observed in the overtone spectrum of *cis-cis* HOONO. Our CRDS measurement demonstrates that the origin band of the first overtone measured in direct absorption is only slightly narrower than the same band detected by action spectroscopy. Fry *et al.*[6] noted that the width of the $2\nu_{OH}$ overtone origin band in the action spectrum (at 6365 cm^{-1}) is $\approx$50% broader than a simulated rotational contour. The laser linewidth in both cases was $\sim$4 cm^{-1}. Thus, the width of the $2\nu_{OH}$ overtone origin band at room temperature is intrinsic to absorption in the overtone band and is not a consequence of using action spectroscopy.

Such broadening may have many causes in an action spectrum: dissociation lifetime broadening, inhomogeneous broadening (especially for bands below D_0, which are exclusively hot bands), or IVR. Since we now find that the linewidth is similar in the direct absorption spectrum, we conclude that the $2\nu_{OH}$ origin band of *cis-cis* HOONO is broadened predominantly by IVR processes.

In contrast, for the *trans-perp* HOONO isomer, the action spectrum of the overtone is fit well by a simulated rotational contour.[6] The difference in widths of the *cis-cis* HOONO versus *trans-perp* HOONO overtone bands indicates that IVR is faster in *cis-cis* HOONO. IVR may be facilitated in *cis-cis* HOONO by the presence of the intramolecular hydrogen bond and the strong stretch-torsion coupling. In *trans-perp* HOONO, the OH bond is out of plane and less likely to relax quickly.

VII. CONCLUSIONS

We report the results of a theoretical and experimental investigation of the dynamics that lead to the observed intensity pattern in the OH first overtone action spectrum of *cis-cis* HOONO. We find that coupling of the OH stretch to the HOON torsion and quantum yield effects are primarily responsible for the features seen in the action spectrum.

Theoretical calculated absorption and action spectra, and experimental measurement of the direct absorption spectrum of *cis-cis* HOONO, confirm that the $2\nu_{OH}$ origin band lies below D_0 and is therefore suppressed in the action spectrum.

We are able to account semiquantitatively for most of the features in the action spectrum and their relative intensities, despite the reduced dimensionality of the calculation. Only one major band, at 6730 cm^{-1}, is not predicted and likely involves other vibrations not treated here. Levels with torsional excitation up to $n=6$ contribute to the spectrum, indicating that perturbation theory is unlikely to describe completely the action spectrum.

The *cis-perp* geometry plays an important role in the spectroscopy of *cis-cis* HOONO. A pileup of torsionally excited $\Delta n=+1$ transitions in a *cis-perp*-like geometry, with an effectively free OH stretch and with large intrinsic intensities, accounts for the strongest band near 7000 cm^{-1} in the action spectrum. This is surprising in light of the high energy of the torsionally excited ground states, but is explained in this study as resulting from a combination of effects: a pileup of multiple states at the *cis-perp* geometry, the anomalously large intrinsic intensity of the OH stretch in the *cis-perp* geometry, and the suppression of the origin band which would otherwise dominate the spectrum.

The calculations are highly sensitive to the dissociation energy and are in excellent agreement with the experimental D_0 determined by Konen *et al.*[18] This resolves the apparent inconsistency between this value of D_0 and the finding of Fry *et al.*[6] that the relative intensities of bands in the $2\nu_{OH}$ region of the action spectrum appear to be independent of temperature. As the temperature is lowered, we predict that torsional hot band intensities in the absorption spectrum decrease significantly. In the action spectrum, this decrease in torsional hot band intensities is nearly exactly matched by a drop in the quantum yield for HOONO dissociation of the bands at lower photon energies, which require additional energy in other modes to dissociate.

The quantity of most relevance in atmospheric chemistry is the branching ratio of HOONO relative to $HONO_2$ in reaction (1). This work suggests an upward adjustment of that branching ratio previously reported by Bean *et al.*[2] The reduced dimensionality of this model does not allow a new quantitative estimate of the branching ratio, but does suggest that further work is required to correctly account for coupling to other modes and to assess the integrated cross section of *cis-cis* HOONO in the fundamental region.

ACKNOWLEDGMENTS

This work was supported by the California Air Resources Board (Contract No. 03-333), the National Science Foundation (NSF Grant Nos. CHE-0200968 and ATM-0432377), and the National Aeronautics and Space Administration Upper Atmospheric Research Program (NASA Grant No. NGT-11657). Experiments were performed in the laboratory of Professor Paul O. Wennberg, and the authors gratefully acknowledge his support and interest. J.L.F. and A.K.M. acknowledge support of NSF Graduate Research Fellowships and a NASA Earth System Science Fellowship. The authors thank the NASA Jet Propulsion Laboratory Supercomputing Project for computer time. They thank Stanley P. Sander, John F. Stanton, Amit Sinha, and Marsha I. Lester for helpful discussions and for sharing unpublished results prior to publication.

[1] S. A. Nizkorodov and P. O. Wennberg, J. Phys. Chem. A **106**, 855 (2002).
[2] B. D. Bean, A. K. Mollner, S. A. Nizkorodov, G. Nair, M. Okumura, S. P. Sander, K. A. Peterson, and J. S. Francisco, J. Phys. Chem. A **107**, 6974 (2003).

[3]H. Hippler, S. Nasterlack, and F. Striebel, Phys. Chem. Chem. Phys. **4**, 2959 (2002).
[4]N. M. Donahue, R. Mohrschladt, T. J. Dransfield, J. G. Anderson, and M. K. Dubey, J. Phys. Chem. A **105**, 1515 (2001).
[5]D. M. Golden, J. R. Barker, and L. L. Lohr, J. Phys. Chem. A **107**, 11057 (2003).
[6]J. L. Fry, S. A. Nizkorodov, M. Okumura, C. M. Roehl, J. S. Francisco, and P. O. Wennberg, J. Chem. Phys. **121**, 1432 (2004).
[7]M. P. McGrath and F. S. Rowland, J. Phys. Chem. **98**, 1061 (1994).
[8]H. H. Tsai, T. P. Hamilton, J. H. M. Tsai, M. van derWoerd, J. G. Harrison, M. J. Jablonsky, J. S. Beckman, and W. H. Koppenol, J. Phys. Chem. **100**, 15087 (1996).
[9]K. N. Houk, K. R. Condroski, and W. A. Pryor, J. Am. Chem. Soc. **118**, 13002 (1996).
[10]R. D. Bach, M. N. Glukhovtsev, and C. Canepa, J. Am. Chem. Soc. **120**, 775 (1998).
[11]K. Doclo and U. Rothlisberger, Chem. Phys. Lett. **297**, 205 (1998).
[12]R. S. Zhu and M. C. Lin, J. Chem. Phys. **119**, 10667 (2003).
[13]J. F. Stanton (private communication).
[14]B. M. Cheng, J. W. Lee, and Y. P. Lee, J. Phys. Chem. **95**, 2814 (1991).
[15]W. J. Lo and Y. P. Lee, J. Chem. Phys. **101**, 5494 (1994).
[16]I. B. Pollack, I. M. Konen, E. X. J. Li, and M. I. Lester, J. Chem. Phys. **119**, 9981 (2003).
[17]J. Matthews, A. Sinha, and J. S. Francisco, J. Chem. Phys. **120**, 10543 (2004).
[18]I. M. Konen, I. B. Pollack, E. X. J. Li, M. I. Lester, M. E. Varner, and J. F. Stanton, J. Chem. Phys. (to be published).
[19]G. Purvis and R. Bartlett, J. Chem. Phys. **76**, 1910 (1982).
[20]K. Raghavachari, G. W. Trucks, J. A. Pople, and M. Head-Gordon, Chem. Phys. Lett. **157**, 479 (1989).
[21]J. D. Watts, J. Gauss, and R. J. Bartlett, J. Chem. Phys. **98**, 8718 (1993).
[22]T. H. Dunning, J. Chem. Phys. **90**, 1007 (1989).
[23]R. A. Kendall, T. H. Dunning, and R. J. Harrison, J. Chem. Phys. **96**, 6796 (1992).
[24]D. E. Woon and T. H. Dunning, J. Chem. Phys. **98**, 1358 (1993).
[25]J. A. Pople, M. Head-Gordon, and K. Raghavachari, J. Chem. Phys. **87**, 5968 (1987).
[26]M. J. Frisch, G. W. Trucks, H. B. Schlegel *et al.*, GAUSSIAN 98, Revision A.9, 1998.
[27]D. T. Colbert and W. H. Miller, J. Chem. Phys. **96**, 1982 (1992).
[28]Z. Bacic and J. C. Light, Annu. Rev. Phys. Chem. **40**, 469 (1989).
[29]See EPAPS Document No. E-JCPSA6-122-009510 for parameters of the potential energy and dipole surfaces. A direct link to this document may be found in the online article's HTML reference section. The document may also be reached via the EPAPS homepage (http://www.aip.org/pubservs/epaps.html) or from ftp.aip.org in the directory /epaps/. See the EPAPS homepage for more information.
[30]J. M. Guilmot, M. Godefroid, and M. Herman, J. Mol. Spectrosc. **160**, 387 (1993).
[31]K. J. Feierabend, D. K. Havey, and V. Vaida, Spectrochim. Acta, Part A **60**, 2775 (2004).